High-Density Single Antibody Electrochemical Nanoarrays

Khalil Chennit,[1] Yannick Coffinier,[2] Shuo Li,[3] Nicolas Clément,[3]* Agnès Anne,[1]* Arnaud Chovin,[1] Christophe Demaille[1]*

[1] Université Paris Cité, CNRS, Laboratoire d'Electrochimie Moléculaire, F-75013 Paris, France.

[2] Institute of Electronics, Microelectronics and Nanotechnology, CNRS, University of Lille, Avenue Poincaré, BP60069, 59652, Villeneuve d'Ascq, France

[3] IIS, LIMMS/CNRS-IIS UMI2820, The University of Tokyo; 4-6-1 Komaba, Meguro-ku Tokyo, 153-8505, Japan

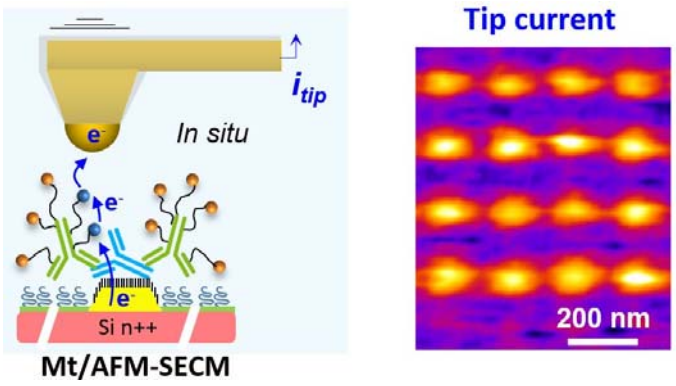

A single-antibody nanodot array is fabricated and electrochemically interrogated, at the ensemble and single nanodot scale.

High-Density Single Antibody Electrochemical Nanoarrays

Khalil Chennit,[1] Yannick Coffinier,[2] Shuo Li,[3] Nicolas Clément,[3](✉) Agnès Anne,[1](✉) Arnaud Chovin,[1] Christophe Demaille[1](✉)

[1] *Université Paris Cité, CNRS, Laboratoire d'Electrochimie Moléculaire, F-75013 Paris, France.*
[2] *Institute of Electronics, Microelectronics and Nanotechnology, CNRS, University of Lille, Avenue Poincaré, BP60069, 59652, Villeneuve d'Ascq, France*
[3] *IIS, LIMMS/CNRS-IIS UMI2820, The University of Tokyo; 4-6-1 Komaba, Meguro-ku Tokyo, 153-8505, Japan*

Received: day month year / **Revised:** day month year / **Accepted:** day month year (automatically inserted by the publisher)

ABSTRACT

The fabrication and electrochemical interrogation of very high density single-antibody nanoarrays is reported. Gold nanodots, 15 nm in diameter, arranged in large (cm^2) square arrays with a pitch of 200 nm, are used as carriers for primary antibodies (Immunoglobulin G, IgGs), further recognized by secondary redox-labeled detection antibodies. Ensemble scale interrogation of the antibody array by cyclic voltammetry, and nanoscale interrogation of individual nanodots by mediator tethered atomic-force electrochemical microscopy (Mt/AFM-SECM), enable the occupancy of nanodots by single antibody molecules to be demonstrated. Experiments involving the competitive adsorption of antibodies of different species onto the nanodots evidence the possibility of using single-antibody nanoarrays for digital electrochemical immunoassays.

KEYWORDS

Single entity electrochemistry, electrochemical digital immunoassays, atomic force electrochemical microscopy, AFM-SECM

1 Introduction

Antibody-based microarrays are analytical devices that have become universal tools for a wide range of bioanalytical applications [1]. They consist of capture antibodies, immobilized on a solid surface in a series of microscopic locations, "spots", forming a regular array. The physical size of the spots, and their spacing, are a few hundred microns, so the term "microbiochips" is classically used, and a spot density in the order of 2000/cm^2 is common [2]. In recent years, the need for mapping complex proteomes has motivated further miniaturization of antibody microchip arrays, toward higher spot densities and smaller spot sizes [2–5]. Antibody *nano*arrays, characterized by spot sizes and inter-spot distances in sub-micron to tens of nanometer range, have become desirable. Several challenges have been identified for the production of such antibody nanoarrays [5]. These include the development of new methodologies for depositing antibodies to form nanoscale spots. Deposition techniques such as dip-pen nanolithography [6–8], surface chemistry patterning by electron or ion beam lithography [9], or nanoimprint lithography [10] have demonstrated their ability to deposit protein nanodomains on surfaces [11], ranging in size from a few tens to a few hundreds of nanometers in diameter. Another strategy is to produce an array of nanometer-sized carriers (nanodots) on which proteins are selectively immobilized by directed self-assembly [12–18]. By matching the size of the nanodots with that of biomolecules, single protein nanoarrays, where each nanodot is occupied by a single protein molecule, have even been fabricated [12,13,16,18]. A second challenge is the development of high resolution microscopy techniques allowing the in-situ reading of antibody nanoarrays. Indeed, the resolution of "classical" fluorescence optical microscopy, routinely used to read microarrays, is diffraction-limited and therefore too low to resolve individual nanodots separated by a few tens of nanometers.

The aim of the present work is to demonstrate the possibility of forming *electrochemically* addressable, high-density, *single*-antibody nanoarrays, by making use of well-defined gold nanodot arrays as antibody displaying platforms and electrochemical atomic force microscopy (AFM-SECM) [19,20], operated in mediator tethered (Mt) – mode [21,22], as a high resolution read-out technique. Albeit interrogation of antibody microarrays by "regular" electrochemical microscopy (SECM) has been previously reported [23–25], SECM read-out of antibody *nano*arrays has never been achieved, in spite of recent progresses in SECM resolution [26,27].

Herein, rabbit antibodies, used as antigens, are selectively adsorbed onto ~15 nm diameter gold nanodots, forming a very high density ($2.5\ 10^9$ dots/cm^2) array on a silicon chip. Molecular recognition by redox-labeled anti-rabbit secondary antibodies makes the antigens electrochemically detectable, both at the ensemble scale by recording cyclic voltammograms at the chip and at the single nanodot scale by Mt/AFM-SECM microscopy. This combined multiscale approach enabled us to quantify and statistically analyze the molecular occupancy of the nanodots by the antigen, and to evidence that single molecule occupancy was achieved. Competitive adsorption of antibodies from different species on the nanodots allowed us to further confirm this result and to demonstrate the possibility of digital reading of the nanoarray.

Address correspondence to Christophe Demaille, demaille@u-paris.fr; Agnès Anne, anne@u-paris.fr; Nicolas Clément, nclement@iis.u-tokyo.ac.jp

2 Results and discussion

2.1 Choice of a model, electrochemically detectable, antigen-antibody system

For the proof-of concept experiments reported here, we made use of a rabbit Immunoglobulin G, (IgG) adsorbed on the nanodots as the single molecular entity (antigen) to be recognized by redox-tagged detection antibody in solution. In this configuration the molecular recognition capabilities of the IgG borne by the nanodot, which may be altered by its adsorption, are not involved. In ensemble scale ELISA (enzyme-linked immunosorbent assays), loss of the recognition capabilities *of some* of the antibodies adsorbed on the bottom of millimeter-sized wells can be ignored due to their multitude, but this is obviously critical at the single antibody scale. This problem can be alleviated by designing immobilization schemes more benign than mere adsorption [28–31], but such a refinement is beyond the scope of the present study. Besides, the configuration used here is reminiscent of the detection step in sandwich ELISA assays, where surface-captured antigens are recognized by (enzyme) labeled secondary antibodies in solution. Yet, here, as a secondary (detection) antibody we made use of a polyclonal goat anti-rabbit IgG labeled by redox active ferrocene (Fc) moieties, borne by flexible linear PEG_{3500} chains. The detection IgG was covalently redox labeled by home-synthesized Fc-PEG-NHS chains, as described previously [32]. MALDI-TOF mass spectrometry of the resulting redox antibodies was used to assess the degree of functionalization of the IgG, evidencing *a single population* of Fc-PEGylated IgG bearing 28 Fc-PEG chains (Fig. S1). This number is close to the estimated ~30 NH_2 groups available at the IgG surface for NHS functionalization, indicating a full “saturating” decoration of the IgGs by the Fc-PEG-chains. As will be evidenced below, knowledge of the composition of the detection antibody population is crucial to the correct interpretation of the Mt/AFM-SECM read-out data.

2.2 Assembly of a high-density single-antibody electrochemical nanoarray

For the assembly of the antibody nanochip we made use of a n^{++} doped silicon surface, bearing a large (cm^2) and very dense array of ultra-flat, gold nanodots produced by a high-speed electron lithography process reported earlier [33] [34]. This process is terminated by a thermal annealing treatment which converts the as-deposited nanodots into truncated octahedron-shaped nanocrystals displaying an atomically flat top [33,35]. The crystals are also half-embedded into the surface and in perfect ohmic contact with the doped silicon material, thus forming an electrically addressable nanoarray [35–37]. For the present study, the fabrication process was set to form nanocrystals 2-3 nm in height and 15 nm in diameter, arranged in a square pattern with 200 nm pitch (Fig. S2). The diameter of the nanocrystals was chosen so as to match the size of IgGs (~15 × 10 × 5 nm^3) [38], favoring the occupancy of nanocrystals by single antibodies**.**

An experimental strategy had to be developed in order to selectively "guide" the adsorption of the primary antibody, but also its subsequent recognition by the secondary antibody, to the surface of the nanodots. This implied blocking the interdot space from non-specific adsorption of these IgGs, while leaving free access to the nanodot surface. It was therefore necessary to modify the interdot area, made of a thin layer of silica, by a molecular layer resistant to protein adsorption. This layer had to be selectively formed on the silica, while sparing the gold surface of the dots, and to be thin enough not to "bury" the few nanometers-tall nanodots.

The nanoarray functionalization protocol presented in Fig. 1 was designed, it was adapted from literature [12,13,39] so as meet with the specific requirements of single-antibody array assembly and electrochemical read-out.

The gold nanodot array, freshly uncovered by HF treatment (see Methods), was exposed to UV-ozone in order to favor the formation of a thin “native” SiO_2 layer over the inter-nanodot region of the Si surface. A protective mercaptohexanol (MCH) layer was then selectively self-assembled on the gold nanodots.

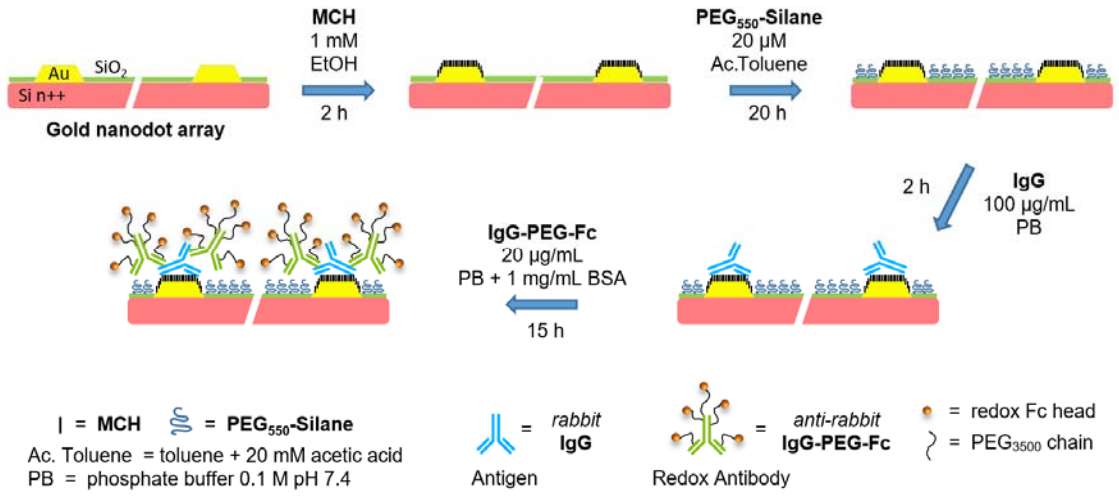

Figure 1 Assembly steps of our model high-density single-antibody nanoarray.

A molecular layer of end-attached PEG chains was then formed in the interdot space, by reaction between the hydroxyl functions present on the SiO_2 layer and methoxy-PEG-triethoxy-silane molecules (550 Da) dissolved in toluene. Such a PEG layer was meant to prevent subsequent non-specific adsorption of proteins in the interdot region. Control experiments, carried out using plain gold surfaces, showed that PEG-silane chains tend to irreversibly adsorb on bare gold, but not on MCH layers, so that protection of the nanocrystals by a MCH layer was indispensable here. The rabbit IgG was then immobilized onto the nanocrystals by mere adsorption. Control experiments confirmed that IgGs are prone to strong (irreversible) adsorption on MCH-coated plain gold surfaces (Fig. S3). In order to make the rabbit IgG electrochemically detectable, the nanoarray was then exposed to the anti-rabbit IgG-PEG-Fc detection antibody. Note that a large concentration of bovine serum albumin (BSA, 1 mg/mL) was present as a carrier protein in the IgG-PEG-Fc solution for preventing its non-specific binding to those nanodots eventually left free of rabbit IgG.

2.3 Cyclic voltammetry characterization of the antibody array

After assembly, the antibody array was mounted as the bottom of a fluid cell, filled with 0.1 M phosphate buffer pH 7.4, connected via the doped silicon surface to a potentiostat and used a working electrode in a three-electrode set up. Cyclic voltammograms (CVs) were then recorded at a scan rate of 1V/s, a typical raw signal thus obtained is reproduced in Fig. 2, blue trace.

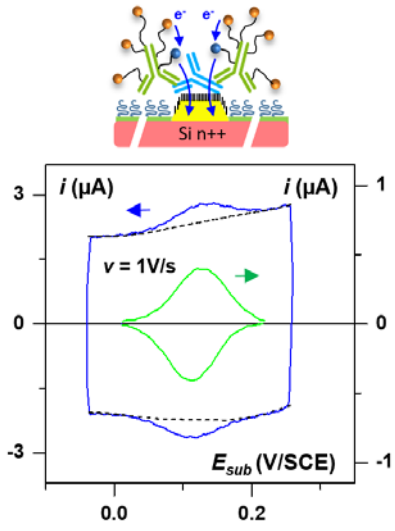

Figure 2 Cyclic voltammetry characterization of a single-antibody array. Rabbit IgG/IgG-PEG-Fc immunocomplexes are selectively immobilized on the gold nanodots. Blue trace: Raw signal. Green trace: voltammogram corrected for capacitive current (dashed line). Scan rate v = 1 V/s. 100 mM phosphate buffer pH 7.4. Top: Schematic showing the oxidation of the ferrocene heads at the nanodots taking place during the anodic scan of the voltammogram.

It displays a pair of well-defined peaks, superimposed to a large capacitive current, which can be easily subtracted to yield the background-corrected faradaic signal displayed in green in Fig. 2. The intensity of the anodic (or cathodic) peak current can be straightforwardly measured, and was found to be proportional to scan rate. The separation between the peaks, was ~10 mV, and the width at half-peak ~90 mV. The half sum of the peak potentials leads to an apparent standard potential, E°, of about 125 mV, which is very close to the standard potential we previously measured for

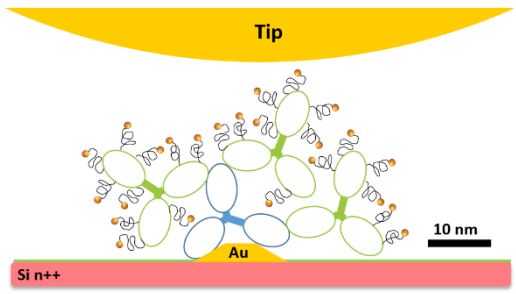

Figure 3 Schematic 2D depiction of a gold nanodot bearing a single adsorbed rabbit IgG, recognized by three IgG-PEG-Fc detection antibodies. The IgGs, gold nanodot and tip are drawn to scale and with their actual geometries (IgG shape and dimensions are from ref. [38]).

Fc-PEG chains directly end-attached to the gold nanodots (130 mV/SCE) [40].

These characteristics, are close to those of an ideal surface signal [41], indicating that ferrocene heads undergo rapid electron transfer, do not interact with each other and experience an essentially aqueous environment similar to the solution. Also note that, when the immunocomplex layer was formed on a gold nanoarray not treated by the PEG-silane, a distorted CV was obtained (Fig. S4). This latter result shows that, in the absence of the PEG layer, IgG-PEG-Fc can adsorb on the inter-nanodot region of the surface and exchange electrons with the doped Si surface through the thin SiO_2 layer, albeit with a slow electron transfer rate. Hence, we can conclude that the voltammogram displayed in Fig. 2 reflects the electrochemical interrogation of Fc heads belonging to immunocomplexes formed specifically on gold nanodots, as represented schematically at the top of Fig. 2.

Integration of the background corrected voltammograms lead to the charge Q = 44 nC, measured under the anodic wave, corresponding to the oxidation of the ferrocene heads of the IgG-PEG-Fc present on the 1.9×10^9 nanodots simultaneously interrogated by CV. This leads to an average number of 145 Fc heads per nanodot, or 5 copies of the IgG-$(PEG\text{-}Fc)_{28}$ species. Throughout our successive experiments, conducted with several different nanodot arrays, we measured Q values corresponding to an average molecular occupancy of the nanodots ranging from 4 to 7 copies of IgG-$(PEG\text{-}Fc)_{28}$. These values seem quite consistent with the respective sizes of the nanodots and IgG, once we take into account that several copies of the polyclonal Fc-PEGylated antibody can recognize each adsorbed primary IgG molecule, Fig. 3.

From such a scaled figure it can also be visualized that, for steric reasons, only 1 or 2 primary IgG molecules can be absorbed onto the nanodots.

Further insights into the molecular occupancy of the nanodots can be brought by *nanoscale* interrogation of the nanoarray, carried out by Mt/AFM-SECM.

2.4 Mt/AFM-SECM tapping mode imaging of the single-antibody array

An antibody nanoarray was prepared following the above described protocol, mounted in the Mt/AFM-SECM cell, and imaged in tapping mode, in 100 mM phosphate buffer pH 7.4. Potentials of E_{tip} = + 0.3 V/SCE and E_{sub} = 0.0 V/SCE were applied to the AFM-SECM probe (tip) and the nanoarray (substrate), respectively. These potentials were selected as they are respectively

very anodic and cathodic compared to the standard potential of the Fc heads. Simultaneously acquired topography and probe current images are reproduced in Fig. 4.

The topography image allows to clearly visualize the dense array of nanodots, forming the expected square array with ~200 nm pitch. The current image shows an identical array of current spots; each spot being associated with a nanodot visible in the topography image. Similarly, *each* nanodot is associated with a current spot. No current signal, apart from low and featureless noise, is measured in the interdot region. We also verified that in the absence of the IgG-PEG-Fc secondary antibody, no spot was visible in the current image (Fig. S5). The same was true when the potential applied to the probe was not anodic enough, or the substrate potential not reducing enough, versus the standard potential of the Fc heads (Fig. S6 and Fig. S7). These results demonstrate that the spots appearing in the current image originate from the detection of Fc-PEG chains carried by IgG-PEG-Fc, as represented schematically in Fig. 4(c): Upon contacting the tip, the Fc heads are oxidized and subsequently reduced back at the nanodot surface. This redox cycling process generates the stationary tip current recorded here. Considering the effective dimension of the PEG_{3500} chains (Flory radius ~5 nm), of the IgGs and of the nanodots (Fig. 3), it is likely that, within the immunocomplexes, electron transport between the nanodot and the tip is ensured jointly by elastic diffusion of the ferrocene heads and electron hopping between neighboring Fc/Fc^+ moieties. This composite charge transport mechanism was previously demonstrated to enable electrons to be conveyed over hundreds of nanometer distances within immunological assemblies [42]. Convolution of the few tens of nanometers-wide "electroactive" immunocomplex with the ~ 100 nm radius tip explains the apparent width of the current spots, of several tens of nanometers.

Thus, qualitatively, the images presented above unambiguously demonstrate the selective decoration of nanodots by IgG/IgG-PEG-Fc immunocomplexes, and their detection by the tip. Analysis of the topography and current image cross-sections enables a more quantitative approach, aiming at better characterizing the molecular occupancy of the nanodots by the immunocomplexes.

Firstly, information can be gained from the height of the nanodots, as measured from the cross-sections of the images taken along the rows, or columns, of nanodots, such those numbered 1 and 3 in Fig. 4. It can be seen from the corresponding profiles, reproduced below the images, that the apparent height of the dots is not homogeneous but rather dispersed. A relevant representation of this dispersion is obtained by plotting histograms of dot height, such as the one presented in Fig. 4(d). The data arise from the analysis of 3 separate images (each histogram color corresponding to one image) and lead to very consistent histograms, peaking around 3 to 5 nm. Considering the global population of ~80 measured nanodots, we arrive at an average nanodot height of 4.5 nm and an absolute standard deviation of 1.9 nm, or a relative standard deviation of 43%. It is relevant to compare these figures to those characterizing the height of bare nanodots, as reported earlier [40]. We then found for undecorated nanodots an average height of 2.3 nm and a relative standard deviation (RSD) of 26%.

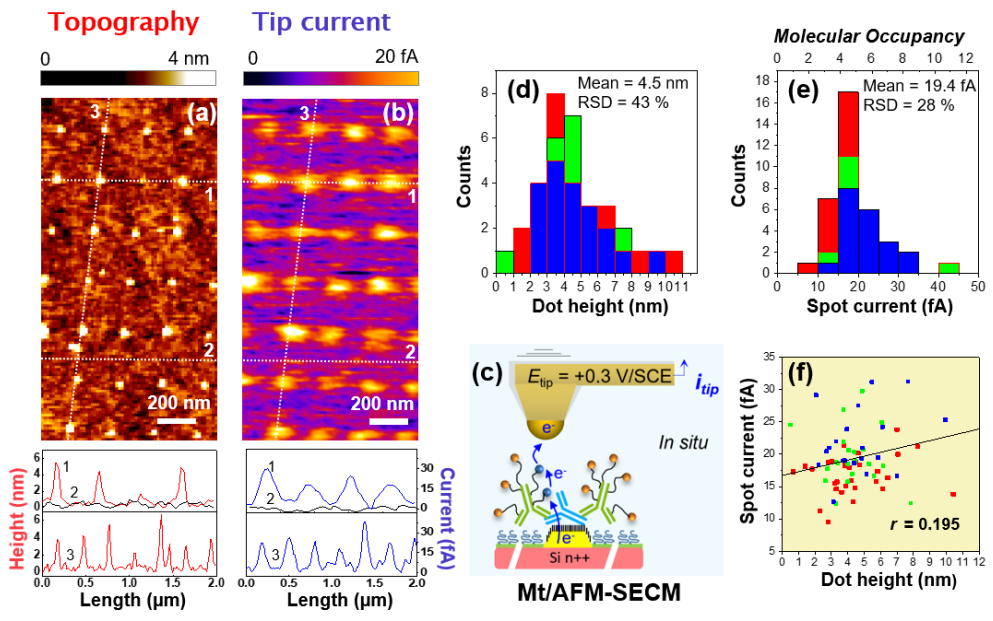

Figure 4 Mt/AFM-SECM images of a single-antibody nanoarray. Rabbit IgGs used as antigens were adsorbed on the nanodots and revealed by an anti-rabbit IgG-PEG-Fc. Left : (a) Topography, (b) tip current images acquired simultaneously. Also shown are cross-sections of the images taken along the dotted lines, identified by their numbers (1, 2, 3). Right : (c) Schematic of the elastic diffusion process coupled to electron hopping generating the probe current. (d) Histograms of nanodot heights, (e) associated spot currents, measured from 3 separate Mt/AFM-SECM images. The red, green, and blue colors refer to each of the images analyzed. The spot current is converted into molecular occupancy (number of IgG-PEG-Fc molecules) using a specific current value of 3.9 fA per IgG-PEG-Fc. (f) Cross-correlation plot where the current of each of the spots is plotted against the height of the corresponding nanodot. The regression line calculated by considering all the measured spots as part of the same population is shown. Imaging medium 100 mM phosphate buffer pH 7.4, E_{sub} = 0.0 V/SCE, E_{tip} = + 0.3 V/SCE.

We can therefore conclude that the presence of the immunocomplex on the surface of the nanodots resulted in doubling the average dot height. The greater dispersion in height of the antibody bearing nanodots, compared to bare dots, can be interpreted as resulting from the variability of the number of antibodies constituting the immunocomplexes. However, we note that the increase in the height of the dots due to the presence of the antibodies is small compared to the size of the IgG (~10 nm). This result suggests that the immunocomplexes, which are flexible and "soft" by nature, are significantly compressed by the combined probe. Yet, such a compression is not damaging since it was possible to image the same nanodots recursively without either the topography of the dots, or the associated spot currents, changing as the scans were performed. Poor "mechanical" sensing of the immunocomplex by the tip also explains the visibly lower apparent diameter of the nanodots in topography images as compared to the width of the current spots (Fig. 4).

We turn now to the measurement of the spot intensity from the current image cross-sections. As can be seen in Fig. 4(b), analysis of vertical cross-sections offers a better accuracy than that of horizontal cross-sections, because the probe current falls more completely to the noise level between each spot. From the analysis of three current images, it is possible to measure the i_{spot} values, the maximum intensity of the spots, for the rather large sample of ~80 dots. The spot current histogram derived from these measurements is shown in Fig. 4(e). It evidences a rather small dispersion of the spot current (RSD = 28 %), centered around a mean value of 19 fA.

The existence of the hopping-based electron propagation mechanism, and the large tip radius (~100 nm) compared to the nanodot diameter, makes very likely that the tip, when positioned over a nanodot, simultaneously addresses all of the Fc-heads of the immunocomplexes, Fig. 3. As a result, the spot current histogram can be interpreted as reflecting the distribution of the number of Fc-PEG chains per nanodot.

A *decisive advantage* of the "saturating" labeling of the IgG by the Fc-PEG-chains, is that, as shown above, the IgG-PEG-Fc exists as a *single* population of PEGylated antibodies so that the number of Fc-PEG and of IgG-PEG-Fc per nanodot are simply proportional to each other (in a 1:28 ratio). In other words, there is here no distribution of the degree of labeling to take into account when interpreting the tip current data statistics [13]. It follows that one can assign the average i_{spot} value of 19 fA to the average number of ~5 IgG-PEG-Fc molecules per nanodot determined above by cyclic substrate voltammetry. This gives a spot current per IgG-PEG-Fc of i^* = 3.9 fA per molecule, and enables us to directly rescale the spot current histogram presented in Fig. 4(e), into a molecular occupancy histogram representing the statistical distribution of the number of IgG-PEG-Fc per nanodot (top abscissa the figure). We see that more than 71% of the nanodots carried 2-5 IgG-PEG-Fc molecules, and only 20% more than 6.

As discussed above, the polyclonal character of Fc-PEGylated IgG makes recognition of the adsorbed primary antibody by several IgG-PEG-Fc molecules very likely. Because of steric hindrances, one can reasonably estimate that ~ 3-4 IgG-PEG-Fc can at most bind to a single adsorbed IgG (Fig. 3). We can therefore state that the majority of nanodots carried a single (or eventually two) molecule(s) of adsorbed primary antibody, so that an electrochemically addressable single-antibody array was indeed assembled here.

It is interesting to see if there is a direct correlation between the height of the spots measured from the topography image and the intensity of the corresponding spots. To do this, a cross-correlation plot can be constructed, where the spot current associated with each nanodot is plotted against the dot height, Fig. 4F. One can observe that the cloud of points thus obtained is relatively dispersed, but that the regression line describing it is ascending. If we admit a proportionality between the spot current and the number of IgG-PEG-Fc, this later result would point to a correlation between the apparent dot height and occupancy. Yet, the large dispersion of the data around the i_{spot} *vs.* height regression line suggests that other random parameters, such as the diameter of the bare nanodots, characterized by a 20 % distribution [33], also sensibly modulate the nanodot molecular occupancy in a way that only the tip current measurement can capture.

2.4 Competitive adsorption of antibodies of different species onto nanodots

In order to confirm achievement of single antigen molecule occupancy of the nanodots, a PEG-protected nanodot array was exposed to a 1 : 3 mixture of rabbit : goat primary IgGs, to allow random competitive adsorption of the antibodies on the nanodots (keeping the total primary IgG concentration constant). The array was then left in contact with the anti-rabbit IgG-PEG-Fc detection antibody, and imaged in situ by tapping mode Mt/AFM-SECM. The topography and current images thus obtained are shown in Fig. 5.

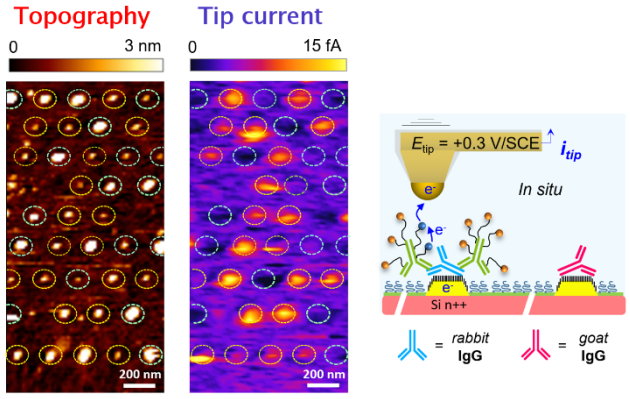

Figure 5 Mt/AFM-SECM images of a single-antibody nanoarray. Rabbit and goat IgGs, used as antigens, were competitively adsorbed on the nanodots from a 1:3 molar ratio solution and revealed by an anti-rabbit IgG-PEG-Fc. Topography and tip current images were acquired simultaneously. 100 mM phosphate buffer pH 7.4, E_{sub} = 0.0 V/SCE, E_{tip} = + 0.3V/SCE.

The topography image shows the presence of the expected regularly spaced nanodots, with only a few missing. Numerous current spots can be seen in the associated current image, each corresponding to a nanodot. However, unlike what was observed above, a significant number of the nanodots visible in the topography image are not associated with any measurable current in the topography image (those are circled in green in Fig. 5). More precisely 17 out of the 39 nanodots (~43 %) did not give rise to a tip current, i.e. did do not carry Fc heads. This result is incompatible with a scenario where nanodots would be occupied by significantly more than one IgG. Indeed, in such a case random co-absorption of goat and rabbit IgGs would have simply resulted in a lower number of IgG-PEG-Fc per dot, since goat IgGs cannot be recognized by the Fc-PEGylated goat IgG, and therefore in a simple decrease of the intensity of the spots. At the opposite, if the

nanodots could each accommodate a single IgG molecule then they would be expected to be either in a “on” or “off” state (i.e. give rise to a tip current or not), depending on whether they bear a rabbit or a goat IgG. Hence, our observation of a significant population of “off” dots supports the single IgG occupancy of the nanodots. The fact that the “on” : “off” ratio observed here (~1:1) for the nanodots differs from the 1:3 rabbit IgG:goat IgG molar ratio of the adsorption solution could be explained by a lower affinity of goat IgG compared to rabbit IgG for adsorption on MCH-coated gold.

The above result opens the way to using our single-antibody nanoarrays for digital immunoassays, where the concentration of a sought protein in solution is quantified by counting the proportion of “on” spots, rather than by the spot intensity. This is very promising since digitizing array-based assays can increase their sensitivity by several orders of magnitude [10,43,44].

3 Conclusions

We have demonstrated the fabrication and multiscale interrogation of an electrochemically addressable, large, high-density, single-antibody nanoarray. A multi-step surface functionalization process enabled the selective immobilization of antibodies on nanodot carriers whose diameter (15 nm) is meant to match the size of IgG molecules. The intended single IgG molecule occupancy of the nanodots was assessed, at the ensemble scale by CV and at the individual nanodot scale by Mt/AFM-SECM. It was shown that our single-antibody nanoarray platform is ready to serve as a basis for digital immunoassays. More generally the present work is an illustration of how single entity (nanodot, antibody) electrochemistry can open new perspectives in bioanalytical science.

4 Materials and methods

4.1 Biological Material.

All the antibodies (Immunoglobulin G, IgG), and bovine serum albumin (BSA, IgG free grade) were from Jackson immunoresearch.

4.2 Chemicals.

The Fc-PEG-NHS derivative used for the Fc-PEG labeling of the goat anti-rabbit detection antibody (IgG) was home-synthesized as described previously [45]. Methoxy-PEG-triethoxy-silane 550 Da (PEG_{550}-Silane) used to PEGylate the nanodot arrays was a Nanocs product. 6-Mercapto-1-hexanol (MCH), toluene, and acetic acid were from Sigma Aldrich and used as received. All aqueous solutions were prepared with double-deionized water (18.2 MΩ cm^{-1} resistivity). A 100 mM phosphate buffer pH 7.4 was used to prepare all the antibody solutions. 2 mg/mL BSA was added to the IgG-PEG-Fc solution, to prevent its non-specific adsorption on gold nanodots, together with 0.1 % sodium azide as a preservative.

4.3 Preparation and MALDI-TOF MS characterization of the redox secondary antibody, IgG-PEG-Fc.

Fc-PEG chains were covalently conjugated to goat anti-rabbit IgG by reacting the NHS activated ester of a home synthesized NHS-PEG_{3500}-Fc chain with the amino groups of the IgG species, as previously described [32]. A 100 molar excess of Fc-PEG-NHS over IgG was used (IgG:NHS of 1:100), resulting in saturating attachment of Fc-PEG chains to the surface-exposed NH_2 of the IgG. MALDI-TOF MS analysis of the purified PEGylated IgG revealed a single population of IgG-PEG-Fc chains with 28 Fc-PEG chains per IgG (see Supporting Information) [46].

4.4 Nanoarray fabrication.

Gold nanocrystal arrays were fabricated on a highly-doped n^{++} silicon substrate, as described previously [33],[34]. As a final fabrication step, thermal annealing at 260°C lead to the formation of facetted gold nanocrystals. As a result of this thermal treatment, the base of the gold nanocrystals was buried in the silicon substrate; some silicon atoms also diffused over the gold. Once exposed to air, the dots were thus covered with a thin silicon dioxide layer which needed to be removed before the nanochip was used.

4.5 Formation of the single-antibody nanoarray.

Just before use, the nanoarray surface was treated by HF (1%, 2 min) to remove the thin SiO_2 layer covering the gold nanodots. The surface was then rinsed with ethanol, water, and dried under N_2. It was subsequently exposed to 30 min UV-ozone cleaning, to promote the formation of pendant hydroxyl functions, crucial for the PEGylation step. After that, the surface was immersed for 2 h in a 1mM solution of mercaptohexanol (MCH) in ethanol. After rinsing with ethanol and toluene, the nanoarray was immersed in a toluene solution containing 20 µM methoxy-PEG-triethoxy-silane (550 Da) and 20 mM acetic acid. The mPEG-silane concentration was kept low in order to avoid polymerization reactions, the reaction time was 20h at room temperature. The PEG-protected surface was thoroughly rinsed with toluene, ethanol then water and mounted in a O-ring fluid cell. The cell was immediately filled with a 100 µg/mL solution of the primary IgG (rabbit IgG or a mixture of rabbit and goat IgGs), prepared in phosphate buffer. Spontaneous adsorption of the IgG on the gold nanodots was left to proceed for 2 h. After rinsing with buffer, the surface was exposed overnight to a 20 µg/mL solution of the IgG-PEG-Fc containing 2 mg/mL BSA. This step was carried out under an Argon atmosphere to prevent oxidative damage/desorption of the thiol and PEG-silane layers. After thorough rinsing with buffer, the antibody nanoarray was ready for immediate *in-situ* characterization.

4.6 CV and AFM-SECM experiments.

The O-ring electrochemical fluid cell was equipped with a platinum coil (counter electrode) and a home-prepared polypyrrole-coated platinum wire (reference electrode), the nanoarray being the working electrode (substrate). All potentials are given *vs*. KCl saturated calomel electrode (SCE). A home-made bipotentiostat was used to record substrate CVs.

In situ tapping mode Mt/AFM-SECM imaging was carried out using a Nanowizard II microscope (JPK, Germany). The AFM-SECM probes (tips) were home-prepared from 60 µm diameter, etched, flattened and insulated gold wires, as detailed previousl [47]. They were characterized by a spring constant in the order of 1-5 nN/nm, a flexural frequency of ~ 2.5 kHz and a typical tip radius of ~100 nm. A setpoint amplitude corresponding to ~80 % of the free oscillation amplitude of the probe was used for imaging (i.e. 20 % damping). The bipotentiostat was used to impose and control independently the potential of the combined

AFM-SECM probe and that of the nanochip to be imaged, and also to record the tip current. A 10 Hz low-pass analogue filter was used to denoise the tip current signal. Slow image scan rates (0.2-0.3 Hz) were employed to avoid distortion of the current image by the filter. Little or no numerical post-filtering was applied to the images.

Acknowledgements

This work has benefited from the facilities and expertise of the Mass Spectrometry platform of ICSN, Institut de Chimie des Substances Naturelle, (Vincent Guérineau, CNRS, Gif-sur-Yvette, France,– **http://icsn.cnrs.fr**).

Electronic Supplementary Material: Supplementary material (Protocol for Fc-PEG labeling of the goat anti-rabbit IgG and MALDI-TOF characterization of the resulting IgG-PEG-Fc. Scanning electron microscopy images of the nanocrystal arrays. CV characterizations of IgG/IgG-PEG-Fc immunolayers assembled on plain MCH-coated gold and on non-PEG protected nanodot array surfaces. Mt/AFM-SECM imaging of single-antibody nanoarrays: Control experiments) is available in the online version of this article at http://dx.doi.org/10.1007/s12274-***-****-* (automatically inserted by the publisher).

References

[1] Z. Chen, T. Dodig-Crnković, J. M. Schwenk, S. Tao, *Clin. Proteomics* **2018**, *15*, 7.

[2] C. Wingren, C. A. K. Borrebaeck, *Drug Discov. Today* **2007**, *12*, 813–819.

[3] C. A. K. Borrebaeck, C. Wingren, *J. Proteomics* **2009**, *72*, 928–935.

[4] S. Ghatnekar-Nilsson, L. Dexlin, C. Wingren, L. Montelius, C. A. K. Borrebaeck, *Proteomics* **2007**, *7*, 540–547.

[5] L. Petersson, M. Coen, N. A. Amro, L. Truedsson, C. A. K. Borrebaeck, C. Wingren, *Bioanalysis* **2014**, *6*, 1175–1185.

[6] K. B. Lee, S. J. Park, C. A. Mirkin, J. C. Smith, M. Mrksich, *Science (80-.).* **2002**, *295*, 1702–1705.

[7] J.-M. Nam, S. W. Han, K.-B. Lee, X. Liu, M. A. Ratner, C. A. Mirkin, *Angew. Chemie Int. Ed.* **2004**, *43*, 1246–1249.

[8] M. Lynch, C. Mosher, J. Huff, S. Nettikadan, J. Johnson, E. Henderson, *Proteomics* **2004**, *4*, 1695–1702.

[9] A. Bruckbauer, D. Zhou, D.-J. Kang, Y. E. Korchev, C. Abell, D. Klenerman, *J. Am. Chem. Soc.* **2004**, *126*, 6508–6509.

[10] G. Zhou, S. Bergeron, S. Ricoult, D. Juncker, in *2013 Transducers Eurosensors XXVII 17th Int. Conf. Solid-State Sensors, Actuators Microsystems (TRANSDUCERS EUROSENSORS XXVII)*, **2013**, pp. 2783–2786.

[11] J. D. Hoff, L. J. Cheng, E. Meyhöfer, L. J. Guo, A. J. Hunt, *Nano Lett.* **2004**, *4*, 853–857.

[12] M. Palma, J. J. Abramson, A. A. Gorodetsky, E. Penzo, R. L. Gonzalez, M. P. Sheetz, C. Nuckolls, J. Hone, S. J. Wind, *J. Am. Chem. Soc.* **2011**, *133*, 7656–7659.

[13] H. Cai, H. Wolfenson, D. Depoil, M. L. Dustin, M. P. Sheetz, S. J. Wind, *ACS Nano* **2016**, *10*, 4173–4183.

[14] M. Wiesbauer, R. Wollhofen, B. Vasic, K. Schilcher, J. Jacak, T. A. Klar, *Nano Lett.* **2013**, *13*, 5672–5678.

[15] R. Schlapak, J. Danzberger, T. Haselgrübler, P. Hinterdorfer, F. Schäffler, S. Howorka, *Nano Lett.* **2012**, *12*, 1983–1989.

[16] J. Chai, L. S. Wong, L. Giam, C. A. Mirkin, *Proc. Natl. Acad. Sci.* **2011**, *108*, 19521–19525.

[17] H. Tran, K. L. Killops, L. M. Campos, *Soft Matter* **2013**, *9*, 6578–6586.

[18] L. Shen, A. Garland, Y. Wang, Z. Li, C. W. Bielawski, A. Guo, X.-Y. Zhu, *Small* **2012**, *8*, 3169–3174.

[19] J. V. Macpherson, P. R. Unwin, *Anal. Chem.* **2000**, *72*, 276–285.

[20] A. Kueng, C. Kranz, A. Lugstein, E. Bertagnolli, B. Mizaikoff, *Angew. Chemie - Int. Ed.* **2003**, *42*, 3238–3240.

[21] A. Anne, E. Cambril, A. Chovin, C. Demaille, *Anal. Chem.* **2010**, *82*, 6353–6362.

[22] A. Anne, A. Chovin, C. Demaille, M. Lafouresse, *Anal. Chem.* **2011**, *83*, 7924–7932.

[23] H. Shiku, T. Matsue, I. Uchida, *Anal. Chem.* **1996**, *68*, 1276–1278.

[24] B. R. Horrocks, G. Wittstock, in *Scanning Electrochem. Microsc. Second Ed.* (Eds.: A.J. Bard, M. V. Mirkin), CRC Press, Boca Raton, **2012**, pp. 317–378.

[25] F. Conzuelo, A. Schulte, W. Schuhmann, *Proc. R. Soc. A Math. Phys. Eng. Sci.* **2018**, *474*, 20180409.

[26] C. L. Bentley, J. Edmondson, G. N. Meloni, D. Perry, V. Shkirskiy, P. R. Unwin, *Anal. Chem.* **2019**, *91*, 84–108.

[27] M. V. Mirkin, T. Sun, Y. Yu, M. Zhou, *Acc. Chem. Res.* **2016**, *49*, 2328–2335.

[28] A. Kausaite-Minkstimiene, A. Ramanaviciene, J. Kirlyte, A. Ramanavicius, *Anal. Chem.* **2010**, *82*, 6401–6408.

[29] N. Tajima, M. Takai, K. Ishihara, *Anal. Chem.* **2011**, *83*, 1969–1976.

[30] N. G. Welch, J. A. Scoble, B. W. Muir, P. J. Pigram, *Biointerphases* **2017**, *12*, 02D301.

[31] S. Gao, J. M. Guisán, J. Rocha-Martin, *Anal. Chim. Acta* **2022**, *1189*, 338907.

[32] A. Anne, C. Demaille, J. Moiroux, *J. Am. Chem. Soc.* **1999**, *121*, 10379–10388.

[33] N. Clément, G. Patriarche, K. Smaali, F. Vaurette, K. Nishiguchi, D. Troadec, A. Fujiwara, D. Vuillaume, *Small* **2011**, *7*, 2607–2613.

[34] J. Trasobares, F. Vaurette, M. François, H. Romijn, J. L. Codron, D. Vuillaume, D. Théron, N. Clément, *Beilstein J. Nanotechnol.* **2014**, *5*, 1918–1925.

[35] K. Smaali, S. Desbief, G. Foti, T. Frederiksen, D. Sanchez-Portal, A. Arnau, J. P. Nys, P. Leclère, D. Vuillaume, N. Clément, *Nanoscale* **2015**, *7*, 1809–1819.

[36] K. Smaali, N. Clément, G. Patriarche, D. Vuillaume, *ACS Nano* **2012**, *6*, 4639–4647.

[37] J. Trasobares, J. Rech, T. Jonckheere, T. Martin, O. Aleveque, E. Levillain, V. Diez-Cabanes, Y. Olivier, J. Cornil, J. P. Nys, R. Sivakumarasamy, K. Smaali, P. Leclere, A. Fujiwara, D. Théron, D. Vuillaume, N. Clément, *Nano Lett.* **2017**, *17*, 3215–3224.

[38] L. F. Pease, J. T. Elliott, D.-H. Tsai, M. R. Zachariah, M. J. Tarlov, *Biotechnol. Bioeng.* **2008**, *101*, 1214–1222.

[39] H. Agheli, J. Malmström, E. M. Larsson, M. Textor, D. S. Sutherland, *Nano Lett.* **2006**, *6*, 1165–1171.

[40] K. Chennit, J. Trasobares, A. Anne, E. Cambril, A. Chovin, N. Clément, C. Demaille, *Anal. Chem.* **2017**, *89*, 11061–11069.

[41] E. Laviron, *J. Electroanal. Chem.* **1979**, *101*, 19–28.

[42] A. Anne, C. Demaille, J. Moiroux, *J. Am. Chem. Soc.* **2001**, *123*, 4817–4825.

[43] L. Cohen, D. R. Walt, *Annu. Rev. Anal. Chem.* **2017**, *10*, 345–363.

[44] L. Cohen, D. R. Walt, *Chem. Rev.* **2019**, *119*, 293–321.

[45] A. Anne, J. Moiroux, *Macromolecules* **1999**, *32*, 5829–5835.

[46] T. O. Paiva, K. Torbensen, A. N. Patel, A. Anne, A. Chovin, C. Demaille, L. Bataille, T. Michon, *ACS Catal.* **2020**, *10*, 7843–7856.

[47] J. Abbou, C. Demaille, M. Druet, J. Moiroux, *Anal. Chem.* **2002**, *74*, 6355–6363.

Electronic Supplementary Material

High-Density Single-antibody Electrochemical Nanoarrays

Khalil Chennit,[1] Yannick Coffinier,[2] Shuo Li,[3] Nicolas Clément,[3](✉) Agnès Anne,[1](✉) Arnaud Chovin,[1] Christophe Demaille[1](✉)

[1] *Université Paris Cité, CNRS, Laboratoire d'Electrochimie Moléculaire, F-75013 Paris, France.*
[2] *Institute of Electronics, Microelectronics and Nanotechnology, CNRS, University of Lille, Avenue Poincaré, BP60069, 59652, Villeneuve d'Ascq, France*
[3] *IIS, LIMMS/CNRS-IIS UMI2820, The University of Tokyo; 4-6-1 Komaba, Meguro-ku Tokyo, 153-8505, Japan*

Supporting information to DOI 10.1007/s12274-****-****-* (automatically inserted by the publisher)

- **Fc-PEG labeling of the goat anti-rabbit IgG**

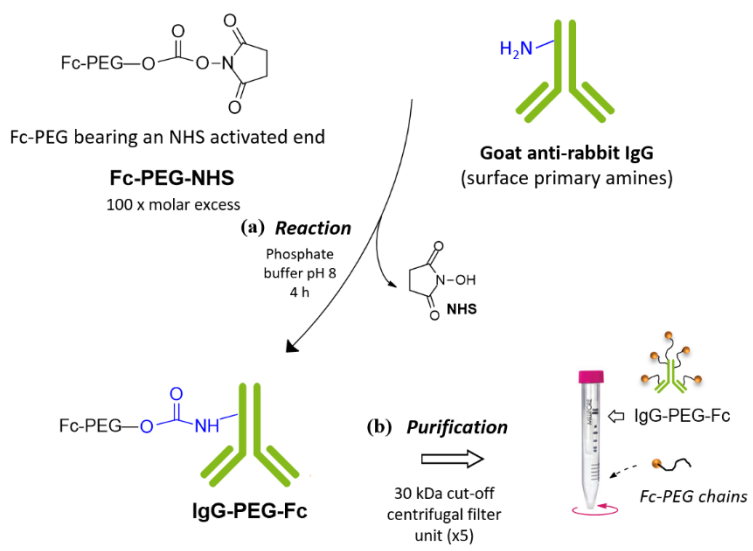

Scheme S1. Fc-PEGylation and purification of the goat anti-rabbit IgG to produce the IgG-PEG-Fc conjugate.

- **MALDI-TOF mass spectrometry characterization of the IgG-PEG-Fc conjugate**

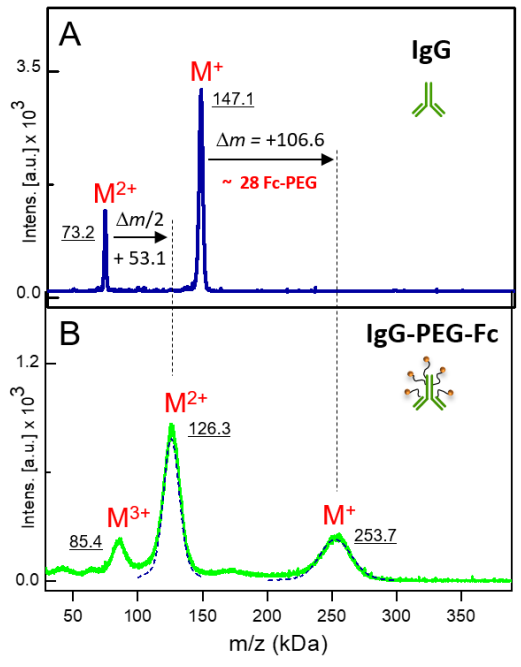

Figure S1. Linear MALDI-TOF mass spectra of the unmodified antibody IgG, (A), and the IgG-PEG-Fc conjugate, (B). The dashed lines in (B) are calculated Gaussian curves with a width at half maximum equal to 28 times that characterizing the mass distribution of Fc-PEG chains. Sinapic acid (Sigma Aldrich) 45 mM in H_2O/acetonitrile/TFA (1/1/0.1) was used as the matrix solution. The IgG protein samples were prepared in 100 mM ammonium acetate at a concentration of 10-20 pmol/µL. Amicon ultra centrifugal filters were used for buffer exchange and protein concentration. The protein sample for MALDI analysis was mixed with the matrix solution at a volume ratio of 1:9 before spotting. Spectrometer: MS UltrafleXtreme (Bruker), operated in positive ion-mode. Acquisition: Vincent Guérineau, ICSN, CNRS, France.

The MALDI-TOF mass spectrum of unmodified goat anti-rabbit IgG (*expected* Mw ~ 150 kDa) is displayed in Figure S1A. It shows two peaks, at m/z values of 147.1 kDa and 73.2 kDa, respectively assigned to the singly positively charged IgG molecular ion, M^+, and to the doubly charged IgG species M^{2+}.

After PEGylation of the IgG with Fc-PEG (Mw = 3800, PDI 1.01), and purification (Scheme S1), the resulting IgG-PEG-Fc bioconjugate was analyzed using MALDI-TOF mass spectrometry. The obtained mass spectrum is shown in Figure S1B. One can observe that the peaks corresponding to the unmodified IgG are absent, indicating that functionalization was exhaustive. The spectrum displays three broad peaks at m/z values of 85.4 kDa, 126.3 kDa and 253.7 kDa. The higher mass peak is assigned to the singly positively charged IgG-PEG-Fc molecular ion, M^+. We note that its mass is 106.6 kDa higher than that of the unmodified IgG. This increase in mass corresponds to the attachment of ~28 Fc-PEG chains (Mw ~3.8 kDa) to the IgG. The two other peaks appear at masses which are almost exactly one-half and one-third the mass of the molecular ion, and are therefore attributed to doubly, M^{2+}, and triply, M^{3+}, positively charged species. The noticeable width of the peaks of the PEG-conjugates reflects the mass distribution of the PEG chain (PDI 1.01). This is evidenced by the fact that the two most notable IgG-PEG-Fc peaks can be reproduced by Gaussian curves with a width at mid-height of 27.5 kDa for M^+ and 14.5 kDa for M^{2+}, corresponding roughly to 28 times that characterizing the mass distribution of the Fc-PEG chains, dashed curves in Figure S1B.

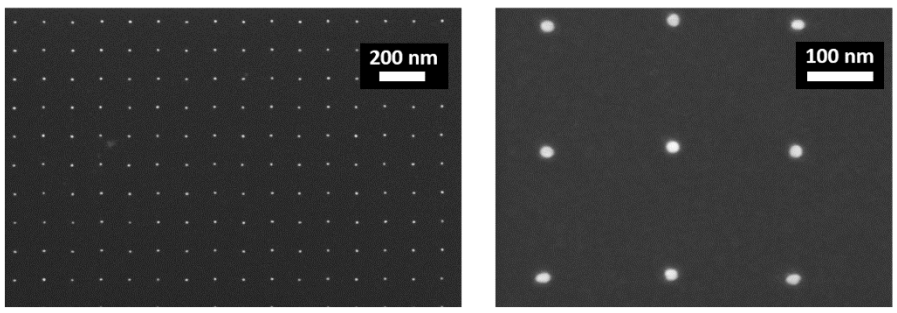

Figure S2. Scanning Electron Microscope (SEM) images of a 200 nm pitch, 15 nm dot diameter, nanocrystal array, as used in this study. SEM is the appropriate technique to assess the diameter as AFM leads to a convolution with the tip. In contrast AFM is the ideal technique to assess the height.

- **IgG/IgG-PEG-Fc immunolayer on a plain MCH-coated gold surface**

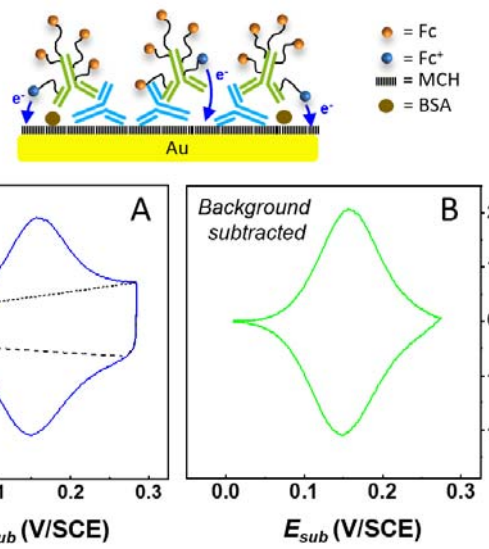

Figure S3. Cyclic voltammetry response of a monolayer of IgG/IgG-PEG-Fc immuno-assembled on a MCH- coated gold electrode. (A) raw signal. Dashed lines represent the capacitive background. (B) Background subtracted signal. 100 mM phosphate buffer pH 7.4

Figure S3 presents a cyclic voltammogram (CV) recorded at a MCH-coated plain gold electrode, bearing a layer of adsorbed rabbit antibody (antigen) recognized by the anti-rabbit IgG-PEG-Fc. Note that recognition was carried out in the presence of a large excess of BSA as a non-specific binding blocking agent. After background subtraction, the CV displays the characteristics of an ideal surface signal, corresponding to fast electron transfer to a surface immobilized species: peak separation is very small (10 mV), peak intensity is proportional to scan rate, peak width at mid height is 91 mV.[i] Half-sum of the forward and backward peak potentials is 152 mV, confirming that the recorded signal is due to the Fc heads borne by the IgG-PEG-Fc ($E° = 150$ mV/SCE),[ii] rapidly exchanging electrons with the gold electrode through the MCH layer.

This result shows that an electrochemically active IgG/IgG-PEG-Fc immunolayer was effectively assembled onto the MCH coated gold surface, evidencing that the high degree of labelling of the anti-rabbit IgG did not alter its molecular recognition capability. Integration of the background subtracted CV yielded a Fc-chain coverage of : $\Gamma_{Fc} = 23 \pm 2$ pmol/cm^2. Since there were 28 Fc-PEG chains per IgG, the IgG-PEG-Fc coverage is $\Gamma_{IgG\text{-}PEG\text{-}Fc} = 0.8 \pm 0.1$ pmol/cm^2, implying that the footprint of the IgG-PEG-Fc on the surface was ~14 nm × 14 nm. Comparing this figure with the estimated footprint of a bare IgG (~ 100 nm)[iii] suggests that the chains attached to the IgG increase its size by about 4 nm, which is quite consistent with the Flory radius of the chains (5 nm).

- **IgG/IgG-PEG-Fc immunolayer on a non-PEG protected nanodot array**

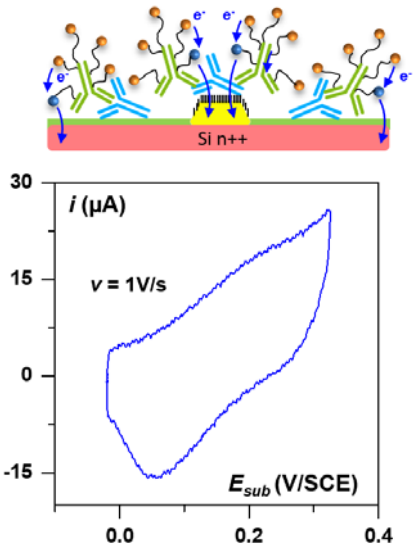

Figure S4. Cyclic voltammetry response of a monolayer of IgG/IgG-PEG-Fc immuno-assembled on a nanodot array surface whose interdot region has not been protected from non-specific adsorption by PEG-silane. 100 mM phosphate buffer pH 7.4

Cyclic voltammograms such as the one reproduced in Figure S4 were recorded at nanodot arrays when the PEG-silanization step was omitted from the IgG/IgG-PEG-Fc immunocomplex assembly process (Figure 1 in the manuscript). These CVs typically displayed an ill-defined anodic peak around + 0.2 V/SCE and a broad cathodic peak in the + 0.05 V/SCE region. Half-sum of the approximate peak potentials was thus ~0.125 V/SCE, confirming that the signal corresponded to the Fc heads. Most importantly, the overall intensity of the CV was more than an order of magnitude higher than that of the signals recorded at PEG-silane protected single-antibody nanoarrays (Figure 2 in the manuscript). It can be concluded that, in the absence of PEG-silane protection, the primary IgG antibody adsorbs strongly in the interdot region of the nanoarray, the IgG-PEG-Fc immuno-complex being able to exchange electrons with the underlying n^{++} doped silicon surface through the thin SiO_2 layer covering it. The sluggishness of such transfer is evidenced by the large peak separation and the distorted aspect of the CV.

- **Mt/AFM-SECM imaging of a nanoarray bearing only the primary antibody**

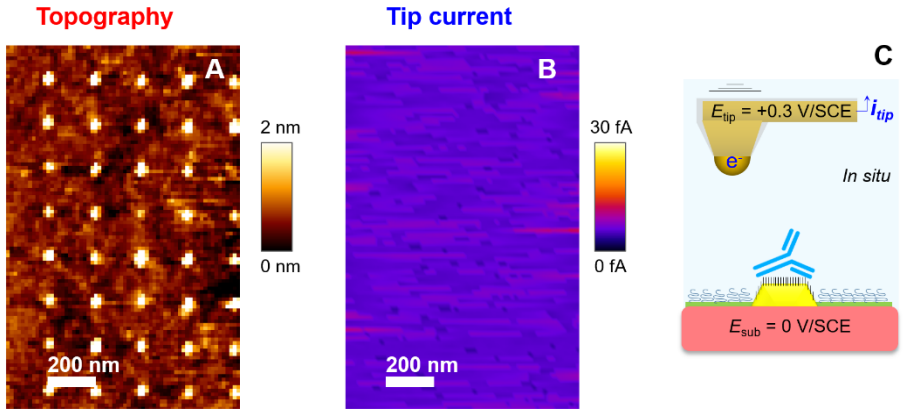

Figure S5. Mt/AFM-SECM images of an antibody nanoarray whose nanodots solely carry primary rabbit antibodies (unlabeled). Topography, (A), and probe current, (B), images acquired simultaneously. (C) Schematic of a primary antibody-decorated dot, the PEG-chain protected silicon surface, and the probe. The imaging medium is 100 mM phosphate buffer pH 7.4. E_{sub} = 0.0 V/SCE, E_{tip} = + 0.3 V/SCE.

Figure S5 presents Mt/AFM-SECM images of a PEG-protected nanodot array surface solely exposed to the primary rabbit antibody, but not to the detection IgG-PEG-Fc redox antibody. As expected, even though nanodots are perfectly visible in topography, they are not associated with any spots in the current image.

- **Mt/AFM-SECM imaging of an antibody nanoarray : effect of tip potential**

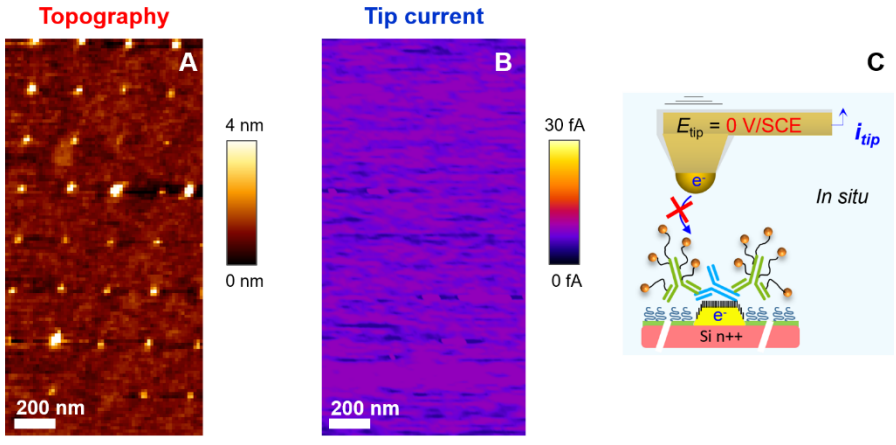

Figure S6. Mt/AFM-SECM images of an antibody nanoarray showing the effect of tip potential on the current image. Topography, (A), and probe current, (B), images acquired simultaneously. The imaging medium is 100 mM phosphate buffer pH 7.4. $E_{tip} = E_{sub} = 0.0$ V/ECS.

Figure S6 shows Mt/AFM-SECM images of a single-antibody nanoarray, acquired with the tip potential too cathodic for oxidation of Fc heads to occur (E_{tip} = 0 V/SCE). As a result, no current spots appear in the current images. By comparing Figure S6 to Figure S5 and Figure 3, one can see that the topography image is unaffected by the tip potential.

- **Mt/AFM-SECM imaging of an antibody nanoarray : substrate potential effect**

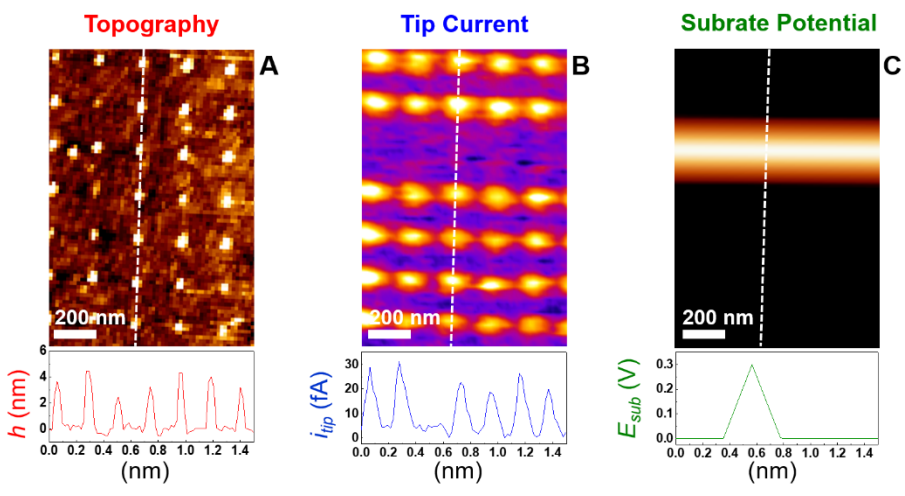

Figure S7. Mt/AFM-SECM images of an antibody nanoarray showing the effect of substrate potential on the spot current. Topography, (A), probe current, (B), and substrate potential, (C), images acquired simultaneously. Also shown are cross-sections of the images taken along the white dashed vertical line. The imaging medium is 100 mM phosphate buffer pH 7.4, E_{tip} = + 0.3 V/SCE.

In Figure S7, a single-antibody nanoarray was imaged by Mt/AFM-SECM, initially with E_{sub} = 0.0 V/ECS and E_{tip} = + 0.3 V/ECS. The image scan direction was from bottom to top. Once the fourth row of nanodots was imaged, the substrate potential was swept progressively anodically and back (at 10 mV/s). It is seen that at the level of the fifth nanodot raw, where E_{sub} ~ +0.3 V/ECS, no current spots were detected, whereas perfectly defined spots could be identified for regions of the image acquired with E_{sub} = 0.0 V/ECS. This result demonstrates that spot current detection is only possible when the surface is sufficiently reducing to regenerate the Fc form of the ferrocene heads oxidized by the probe.

Overall the above results emphasize the specificity of the detection of the immunocomplex *via* the Mt/AFM-SECM tip current.

References

[i] Laviron, E. General Expression of the Linear Potential Sweep Voltammogram in the Case of Diffusionless Electrochemical Systems. J. Electroanal. Chem. 1979, 101, 19–28.

[ii] Anne, A.; Demaille, C.; Moiroux, J. Terminal Attachment of Polyethylene Glycol (PEG) Chains to a Gold Electrode Surface. Cyclic Voltammetry Applied to the Quantitative Characterization of the Flexibility of the Attached PEG Chains and of Their Penetration by Mobile PEG Chains. Macromolecules 2002, 35, 5578–5586.

[iii] Pease, L. F.; Elliott, J. T.; Tsai, D.-H.; Zachariah, M. R.; Tarlov, M. J. Determination of Protein Aggregation with Differential Mobility Analysis: Application to IgG Antibody. Biotechnol. Bioeng. 2008, 101, 1214–1222.

Address correspondence to Christophe Demaille, demaille@u-paris.fr; Agnès Anne, anne@u-paris.fr ; Nicolas Clément, nclement@iis.u-tokyo.ac.jp